Improving solar fuel production performance from H2O and CO2 thermochemical dissociation using custom-made reticulated porous ceria

A. Le Gal, M. Drobek, A. Julbe, Stéphane Abanades

Improving solar fuel production performance from H_2O and CO_2 thermochemical dissociation using custom-made reticulated porous ceria

Alex Le Gal[1], Martin Drobek[2], Anne Julbe[2], Stéphane Abanades[1*]

[1] Processes, Materials and Solar Energy laboratory (PROMES-CNRS) ; 7 rue du Four Solaire ; 66120 Odeillo Font-Romeu ; France

[2] Institut Européen des Membranes (IEM) ; CNRS, ENSCM, Univ Montpellier ; Place Eugène Bataillon ; 34095 Montpellier ; France

***** Corresponding author: stephane.abanades@promes.cnrs.fr

Abstract

Thermochemical CO_2- and H_2O-splitting cycles for sustainable fuel generation were investigated by using custom-made reticulated ceria foams integrated in a solar-heated cavity reactor. A parametric study revealed the suitable conditions to produce H_2/CO with maximum fuel rates and yields per unit mass of redox material. Various operating parameters such as the total pressure during the reduction step, the gas inlet flowrates, the temperature or the reactive gas content during the oxidation step were studied in detail. A series of on-sun experiments including more than 20 cycles under different cycling conditions were carried out with relevant performance repeatability and stability. With a ceria foam reduction temperature in the range 1400-1470°C and a reduction pressure of 103 mbar, the ceria foams produced 281 µmol of H_2 and 332 µmol of CO per gram of material during oxidation below 1000°C under cooling with a maximum production rate of 3.0 mL/min.g and 10.2 mL/min.g, respectively. Direct syngas production was also evidenced during on-sun experiments with simultaneous H_2O- and CO_2-splitting, which yielded a H_2:CO ratio ranging from 0.7 to 1.14. The dual-

scale porous ceria structures were characterized by XRD, SEM, and TGA to confirm material thermal stability during cycling. Finally, optimization of fuel production capacity was achieved by maximizing the total amount of ceria foam loaded into the reactor, yielding 667 mL of CO (409 µmol/g) and 513 mL of H_2 (314 µmol/g) per cycle. A maximum solar-to-fuel efficiency of 10.1% was calculated for CO_2-splitting versus 4.9% for H_2O-splitting cycle. This study thus demonstrated noteworthy fuel production performance in an efficient monolithic reactor under real concentrated solar radiation, from highly-reactive customized ceria foams.

Keywords: *Hydrogen, Syngas, Water splitting, CO_2 conversion, Thermochemical cycles, Concentrated solar energy, Ceria foam.*

1. Introduction

The sustainable production of hydrogen or syngas (H_2+CO mixture) fuel is a major challenge for today's society because it could advantageously replace the consumption of fossil fuels. Innovative solutions must be developed to produce such energy carriers without emitting greenhouse gases or consuming fossil fuel resources. First commercial deployments of sustainable hydrogen fabrication are emerging in 2023 with hydrogen production plants that use renewable electricity from wind energy to produce "green" hydrogen by electrolysis [1]. Other pre-commercial projects focus on hydrogen production from photovoltaic electricity still using electrolysis [2]. Nevertheless, this approach suffers from low overall energy conversion performance due to low power generation efficiency. Alternative solutions to electrolysis from renewable energy sources could be more effective and could allow the production of sustainable hydrogen or syngas with lower production costs. From the proposed multiplicity of alternative pathways, multi-step thermochemical processes using concentrated solar energy appear as a credible route to produce hydrogen or syngas [3],[4],[5]. Two-step thermochemical cycles involving metal oxide redox pairs to split H_2O and/or CO_2 have been investigated for several decades, as reported in numerous review papers [6]-[10]. The thermochemical process involves redox pairs to

dissociate H_2O (or CO_2) molecules into separate streams of H_2 (or CO) and O_2. These cycles are composed of an activation step, consisting of the partial metal oxide reduction (Eq. 1), followed by a hydrolysis step leading to the release of H_2 (or CO) (Eq. 2).

$$M_xO_y \rightarrow M_xO_{y-\delta} + \delta/2\ O_2 \quad (1)$$

$$M_xO_{y-\delta} + \delta\ H_2O\ (+\ \delta\ CO_2) \rightarrow M_xO_y + \delta\ H_2\ (+\ \delta\ CO) \quad (2)$$

The first reaction (partial oxide reduction) is endothermal requiring thermal energy provided by concentrated solar radiation. This reaction occurs at a temperature significantly lower than the direct single-step thermolysis of water (T > 2500°C) but still requires temperatures of about 1400°C achievable with concentrated solar energy. The second reaction (oxidation) is exothermic and requires no solar energy input (provided the temperature is high enough for the reaction kinetics). The conversion efficiency is not limited by any intermediate electricity production step and could theoretically exceed the conversion efficiency of electrolysis [5],[11],[12].

Currently, the measured performance of such processes is still low ($\eta_{solar\text{-}to\text{-}syngas}$ below 5%, defined as the ratio of the higher heating value of the syngas produced to the sum of solar energy input Q_{solar} and any other parasitic energy inputs such as those associated with vacuum pumping and/or inert gas consumption) [13],[14]. Different types of solar thermochemical reactors have been already studied applying ceria as redox material. Some reactors are using moving materials such as the aerosol reactor for the reduction step by indirect heating [15], the moving packed-bed reactor [16], or the rotary-type reactors [17],[18]. Stationary oxides are used in other monolithic reactor concepts such as honeycomb [19], or cavity reactors [20],[21],[22], allowing to proceed both reaction steps in the same reaction chamber. Theoretical investigations on thermodynamics reveal a maximum solar-to-fuel efficiency of 12.9% using ceria [23]. The main limitation to improving efficiency comes from the characteristics of the redox material. Indeed, kinetic [24],[25] or thermodynamic [26],[27] limitations of the currently used redox materials (such as CeO_2, $NiFe_2O_4$ or lanthanum-manganite perovskites $La_xSr_{1-x}MnO_3$) lead to low reduction capability or limited hydrogen or syngas production output per cycle. These fuel

production performances could be increased by using either new materials with improved redox properties (rapid kinetics, high reducibility) and/or by optimizing the operating conditions.

New perovskite formulations or high entropy oxides (HEO) have been studied to find the best-in-class material that will allow a profitable solar thermochemical hydrogen or syngas production. Several review papers have been published on perovskites thermodynamics, design principles and experimental results [28]-[30]. All mention that perovskites can accommodate huge composition space, are thermally stable in the solid phase, and can accept large oxygen non-stoichiometry without phase change. From the broad compositional possibilities, computational calculations and experimental screening studies have identified lanthanum-manganese, lanthanum-cobalt, and yttrium-manganese, together with other dopants, as promising candidate perovskites for solar thermochemical cycles. These perovskites enable a decrease in the reduction temperature to reach a given degree of reduction compared to ceria, but their relatively low reduction enthalpies lead to a lower reactivity for the splitting step. All the reported perovskites need high excess of steam or CO_2 to complete re-oxidation, which negatively impacts the solar-to-fuel efficiency. Regarding high entropy oxides, Zhai et al. reported a high hydrogen production yield of 10.1 mL/g with $(FeMgCoNi)O_x$ [31], and Gao et al. also investigated such a material showing high production yields during microwave-assisted hydrogen production [32],[33]. Within the frame of the American project “HydroGEN: Advanced water splitting materials”, new high entropy perovskite oxides (HEPO) have been studied [34]. This potentially transformative new class of water splitting materials is being investigated with a H_2 yield target of 400 µmol/g operating for 50 one-hour cycles (reduction and oxidation). An experimental screening of new HEO compositions for application in solar thermochemical cycles was also published in 2022 [35].

In addition to the formulation of materials, the improvement of the involved solid/gas reactions could also be achieved by a relevant material shaping. Indeed, by increasing the volumetric absorption of the concentrated solar radiative flux, or by increasing the porosity and the specific surface area, the overall reactivity could be improved. Reticulated foams have shown attractive results with ceria [36]-[41].

Pullar et al. reviewed ceria-based ceramics with designed morphologies and microstructure in 2019 [42]Erreur ! Source du renvoi introuvable. and reported an influence of porosity and microstructure on reactivity, although the comparison is not trivial due to heterogeneity of procedure and experimental conditions (partial pressure pO_2, temperature, time, loaded mass). Ceria fibbers [43],[44], ceria felts [45], reticulated porous ceria [46], ceria microspheres [47] or 3D-ordered microporous ceria [48],[49], have been studied, showing increased amount of produced fuel compared to unshaped ceria powders [50]. Perovskite-coated ceria foams were also found to offer improved CO_2 and H_2O splitting performance [51].

The present study deals with the synthesis and characterisation of custom-made reticulated ceria foams with the aim to improve solar H_2/CO production. A comprehensive study ranging from material synthesis and microstructure optimization to performance testing in a solar reactor under real environmental conditions (high solar flux and high temperatures) is reported, along with the investigation of the impact of the main operating parameters controlling the process. The methods employed to improve materials and solar thermochemical conversion outcome were studied. A detailed parametric study was carried out to determine the main parameters influencing CO_2 and H_2O splitting (Section 3.2). The reactive material for redox cycling was prepared as reticulated porous foams with improved morphology and microstructure suitable for solid-gas reactions and solar radiation absorption. Dual-scale porous ceria structures were synthesized by using the replication method with the addition of filamentous porogens. The pristine redox-active foams were characterized and then cycled in a cavity reactor under concentrated solar irradiation. During the on-sun experimental campaign, numerous operational parameters were investigated and optimized to improve H_2/CO production. Cyclability tests were carried out over several consecutive cycles for splitting CO_2 and H_2O to show performance stability. Process/reactor optimization was a key aspect of the work as the objective was to optimize the fuel productivity and efficiency. Performance/efficiency were evaluated under various operating conditions, closely representative of a real solar process. Results showed that the fuel production rate is greatly affected by various parameters including pressure during reduction,

temperature during oxidation, oxidant mole fraction or oxidant gas flow-rate (Sections 3.2.1 and 3.2.2). Operational strategies can thus be optimized by focusing on tuning these parameters. Processing limitations regarding the simultaneous co-feeding of H_2O and CO_2 for direct syngas production were also unravelled (Section 3.2.3). The amount of loaded material in the reactor was finally optimized for maximum fuel production capacity (Section 3.3). Results were compared to the best-in-class materials in order to confirm that solar fuel production performance can be improved by a relevant material shaping, while optimizing its total loaded amount and cycling conditions.

2. Experimental methods

2.1. Materials synthesis

Reticulated ceramic foams were synthesized using the replication method described elsewhere [52]. An aqueous slurry was first realized with the defined oxide powder, the porogen, and organic additives (see Table 1).

Table 1. Components in the slurry used to make foams via the replication method (the percentages are expressed in relation to the mass and volume of ceria).

Slurry components	Name/composition/provider	Proportion
Raw material	Ceria (Sigma-Aldrich, 99.9%, <5 µm powder)	m
Solvent	Water	m/3
Porogen	Carbon fibbers (Sigrafil® M80-3.0, filaments 7 µm diameter and 80 µm long)	30 vol%
Binder	Polyvinyl alcohol (Mowiol)	1.35 wt%
Dispersant	Dolapix (Zschimmer & Schwarz GmbH)	0.85 wt%

Then, a sacrificial polyurethane template (interconnected open-cell foam with a pore density of 10 ppi) was plunged once into the slurry and dried overnight at room temperature. The as-impregnated foam was then slowly heated up to 1000°C (at 2.5°C/min) to remove the organic components of the foam precursor, and annealed at 1400°C during 3 hours to achieve sintering that provides a mechanical strength to the foam. Polyurethane discs and rings with a diameter of 54 mm and a thickness of 20

147 mm were coated with the slurry described above. Figure 1.a shows the grey colour of the disc before
148 calcination due to the carbon fibbers porogen. After calcination at 1400°C, the foam contains only CeO_2
149 and becomes yellowish (Fig. 1.b). The sintering phenomenon causes a shrinkage of the foam of $15\%_{vol}$.
150 The foams have a final diameter of 46 mm, slightly less than the diameter of the cavity in the solar
151 reactor, therefore suitable for their loading inside the cavity. Optical microscopy was used to
152 characterize the morphology of the foams. The polyurethane template was completely eliminated and
153 left empty spaces inside strands (Fig. 1.c. and 1.d). The optical shadow effect mode permits to observe
154 the porous surface of the foam (Fig. 1.e). Higher magnifications obtained with SEM allow an
155 observation of well-distributed interconnected cylindrical pores of about 80 µm in length and 8 µm in
156 diameter (see Section 3.4). This high porosity, obtained thanks to the porogenic carbon fibbers, should
157 promote the diffusion of gas species inside the struts and thus improve the reactivity in the bulk. The
158 dual scale porosity allows both good penetration of the solar radiative flux and diffusion of gases inside
159 the material. The mass of such ceria foams depends on the thickness of the coating during
160 impregnation. Reticulated ceria discs 46 mm in diameter and 17 mm in height weight approximately
161 30 g. This corresponds to a bulk density of 1.06 g/cm^3. By comparison with the density of ceria ($\rho = 7.13$
162 g/cm^3 – *data from Sigma-Aldrich*), a porosity of 85% is calculated.

163

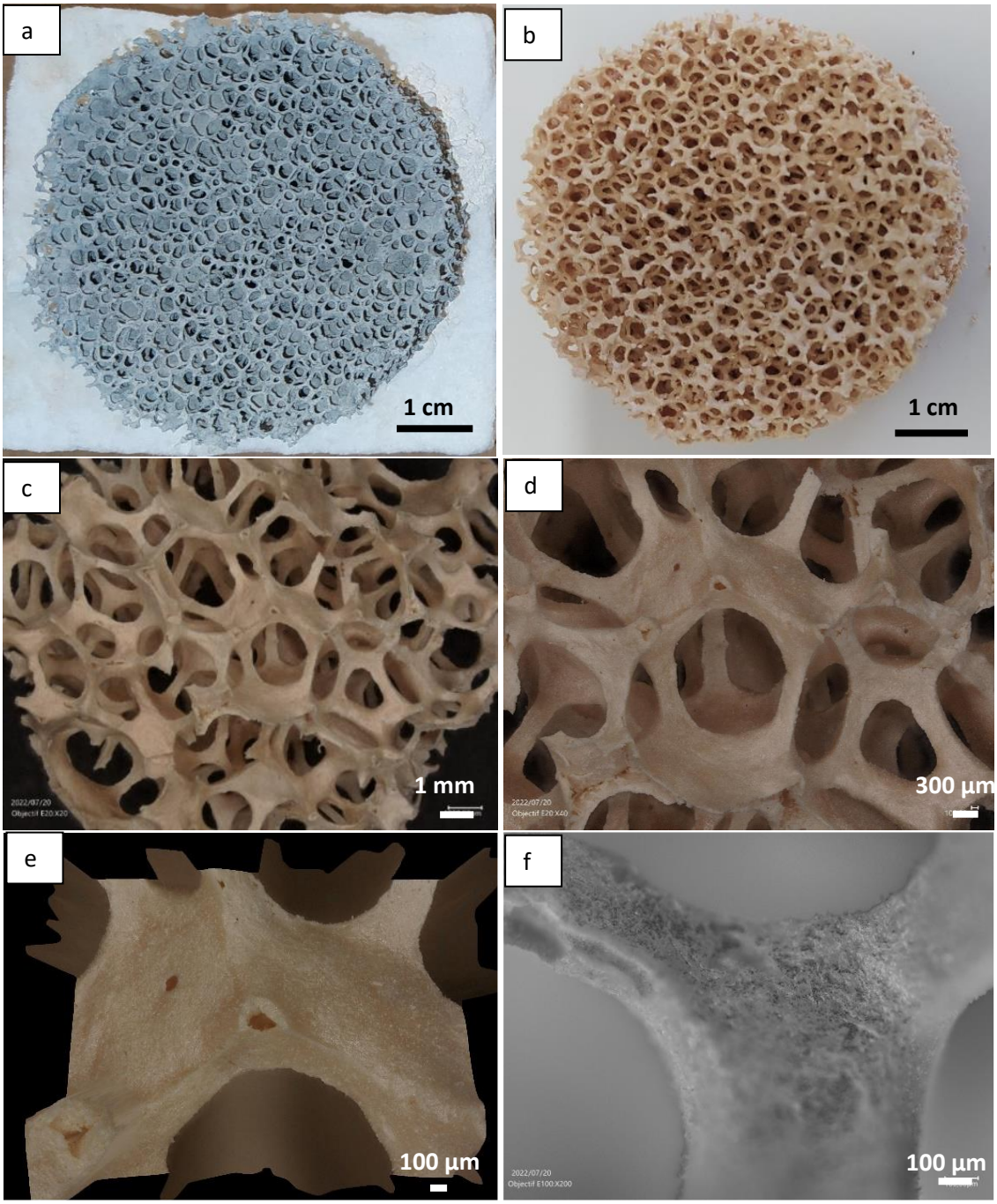

Figure 1. Images of porous CeO_2 foams obtained by the replication method: (a) photograph of the polyurethane foam coated with the slurry before calcination, and (b) after calcination. (c), (d), (e) Optical microscopy of a CeO_2 foam after calcination. (f) Image in shadow effect mode of a foam strand.

2.2 Characterization

The structure and microstructure of the prepared ceria foams were fully characterized with the following series of techniques.

The crystalline structure was studied by X-ray diffraction (XRD) using a Panalytical X'PERT PRO diffractometer with the Cu Kα radiation (αCu = 0.15406 nm, angular range = 20-80°, 2θ, tube current 20 mA, potential 40 kV).

The morphology of the foams was first observed with a Keyence VHX digital microscope equipped with a VHXAnalyser software. In addition, a Field Emission Scanning Electron Microscope (FESEM - Hitachi S4800) was used to observe the microstructure of ceria foams before and after thermochemical cycles.

Thermogravimetric analysis (TGA, SETARAM Setsys Evo 1750) was used to measure the mass variations (amount of oxygen exchanged) associated to the reduction and the oxidation steps of thermochemical cycles. The sample was heated under argon flow (20 mL/min) with a heating rate of 20°C/min up to the selected set-point temperature, and the mass variation was recorded continuously. The successive steps of cycles were carried out at different temperatures (typically 1400°C dwelled for 45 min during the reduction step and 1050°C dwelled for one hour during the CO_2-splitting step) and CO_2 was injected during the oxidation step (50% CO_2 in Ar with a CO_2 flowrate of 10 mL/min).

2.3 Solar reactor

Figure 2 shows a scheme of the solar reactor developed in our previous work [36]. It consists of a cylindrical water-cooled stainless-steel vessel in which an insulated alumina cavity is placed. The reactor is capped with a hemispherical window of transparent Pyrex glass that allows concentrated solar flux to enter the cavity, and that separates the reactive materials and reaction chamber from the outside atmosphere. Three B-type thermocouples are positioned along the height of the cavity in contact with the foam to measure the temperature. A solar-blind pyrometer, placed vertically to the cavity, is used to measure the temperature of the foam in a central point (in the foam cavity at the center of the rings). The T1 thermocouple, which is used as temperature reference, is placed in contact

with the external side of a foam at 20 mm from the bottom of the cavity, whereas the pyrometer measures the temperature in the middle of the foam cavity formed by the rings. Several pressure sensors are fitted to the reactor to monitor the pressure inside the cavity and at the gas inlets. The reticulated foams are positioned in the cavity. The sweep gas (Ar, 99.999% purity, $p_{O2} = 10^{-5}$ bar) can flow from the top of the cavity and/or from the side, and the gas outlet is located under the reactive materials at the cavity bottom. Therefore, the gas flows through the reticulated foams. CO_2 (99.995% purity) and/or steam are injected from the side of the cavity. To produce steam, liquid water is injected through a liquid mass flow controller (range 0-60 g/h) in an alumina capillary connected to the cavity. The liquid water is vaporized before entering the cavity and transported by the inert sweep gas. The gas outlet is connected to an O_2 trace analyser (electrochemical cell) and an H_2 analyser (catharometer) or CO analyser (NDIR sensor) to measure gas concentrations on-line. When co-feeding H_2O and CO_2, a syngas analyser (Emerson XStream) is used to monitor the gas species concentrations continuously and simultaneously (especially H_2 and CO). For the experimental campaign, the reactor is placed at the focus of a vertical-axis solar furnace. A solar concentrator (2 m diameter parabolic dish) of 1.5 kW (thermal) is used to concentrate the solar radiation coming from a sun-tracking heliostat located 30 m below the reactor frame (the reactor thus does not need to be moved as only the heliostat two-axis tracking is used to follow the sun's position). The process heat source is therefore real concentrated solar energy provided by the solar furnace. A shutter is placed between the heliostat and the parabola to control the solar power input during thermochemical cycles. A calibration curve is used to calculate the solar power input as a function of the shutter closing and the DNI (Direct Normal Irradiation). A vacuum pump is used to purge the reactor prior to experiments to remove oxygen and to control the total pressure in the cavity during the cycle reduction step.

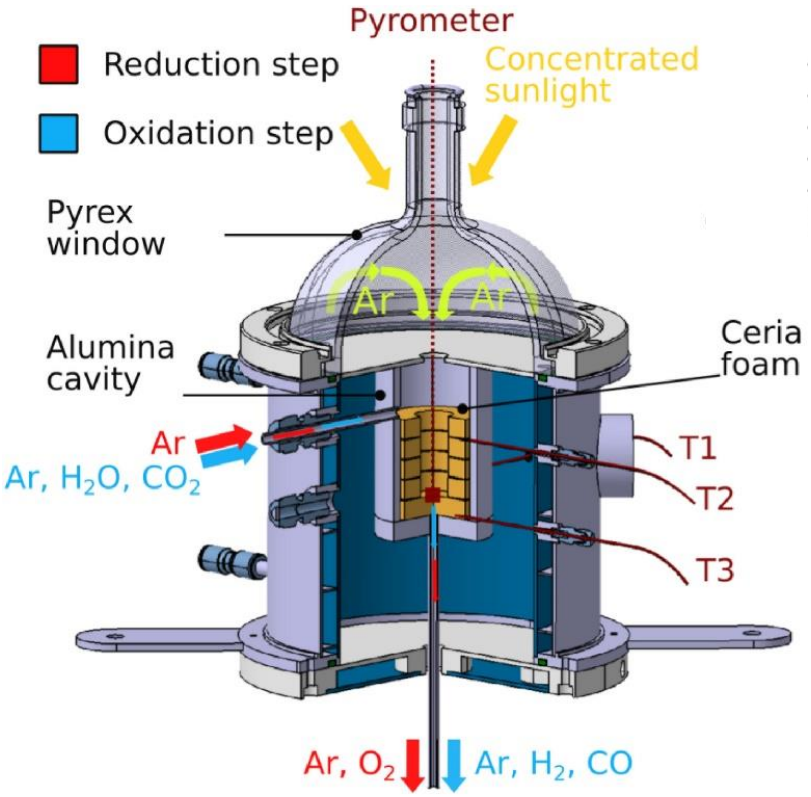

Figure 2. Scheme of the solar reactor.

The experimental protocol is described in the following. Ceria foams are first weighted and placed in the cavity. A full disc is placed at the bottom and two rings are positioned above the disc. The reactor is purged with argon until the oxygen outlet concentration is below 10 ppm. The inert gas flow is regulated at the desired value with a mass flow meter. The total pressure in the reactor is set by using a vacuum pump (p_{O2} depends directly on the reactor total pressure). Then, the ceria foams are gradually heated by opening the shutter of the concentrator until reaching the desired temperature (T1 = 1400°C). This stage corresponds to the reduction step of the cycle and oxygen is continuously released by ceria during heating. Once the temperature is reached, a plateau is maintained. The oxygen concentration decreases until thermodynamic equilibrium of ceria foam reduction is reached (~ 45 min), indicating that the reduction step is completed. In this work, we did not seek to minimize the duration of the reduction step and therefore we rather used sufficiently long durations (slow heating rates with long enough temperature dwells during reduction) to ensure that the O_2 concentration returns to negligible values (thereby ensuring a reduction step close to equilibrium) before proceeding to the oxidation step. Moreover, during reactor heating the solar power input P_{solar} was not at its

nominal value but was gradually increased by opening the shutter to progressively heat the system. The total oxygen release per gram of ceria is calculated by integrating the O_2 concentration in the exhaust gas over the reduction time. It is important to note that the oxygen partial pressure (p_{O2}) during the reduction step is not constant in the reactor and varies greatly between the inlet (inert gas), the ceria foam, and the outlet of the reactor. It further depends on the time-dependent rate of O_2 production from the material (hence on the temperature and heating rate). For the oxidation step, the shutter is then closed to decrease the temperature. The re-oxidation step is carried out under non-isothermal conditions, which means that steam or CO_2 is injected during free cooling (without solar heating) from a defined temperature, but there is no dwell and the temperature drops continuously during this step (about 5 min). The argon and steam/CO_2 flows are regulated to the desired values by using mass flow meters. H_2/CO concentrations in the exhaust gas are recorded on-line and integrated over time to calculate the total H_2/CO production per gram of ceria. Figure 3 shows a schematic representation of the ceria foams in the cavity and different pictures of the solar reactor during the experimental campaign.

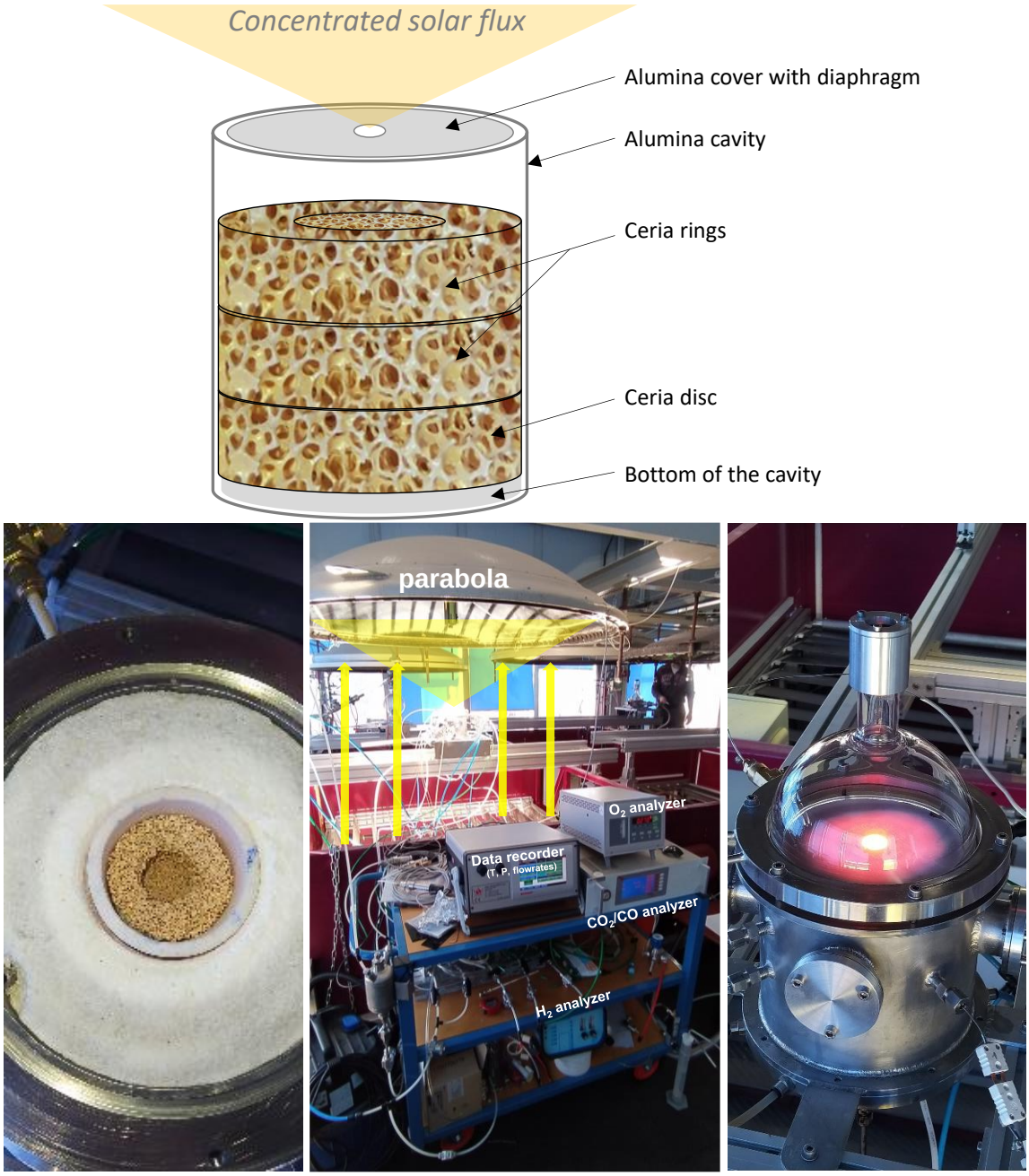

Figure 3. Schematic representation of ceria foams placed in the cavity (top) and pictures of the solar reactor used to characterize the H_2/CO production (bottom).

3. Results and discussion

3.1 Preliminary characterizations of materials

XRD patterns of the crushed foams before and after cycling are presented in Figure 4. The ceria phase is observed and compared to pure ceria powder. The diffraction peaks are sharpened indicating an

increase of the crystallite size caused by the thermal treatment. Crystallite size calculation using the Scherrer formula gives a size of 79 nm for the powder and 106 nm for the foam before and after thermochemical cycling. The size of the crystallites thus remains almost unchanged during the thermochemical cycles. This means that the crystalline domains were stabilized before cycling experiments, thanks to the high temperature of the heat treatment in air during the preparation of the foam, and crystallite sizes did not evolve significantly during cycles.

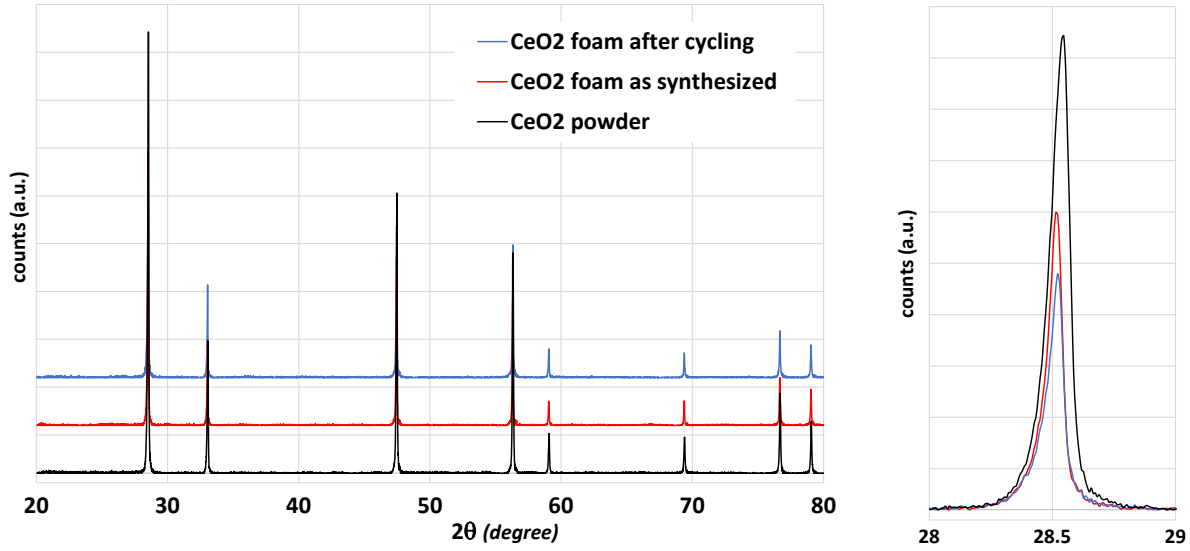

Figure 4. XRD patterns of ceria foams before and after cycling (pure ceria powder is reported for comparison).

Thermogravimetric analysis of both the commercial ceria powder and the derived custom-made ceria foam were carried out (Fig. 5). Two consecutive CO_2-splitting cycles were realized with a reduction temperature of 1400°C and an oxidation temperature of 1050°C. During the reduction steps at 1400°C, the ceria powder released 55 and 54 µmol/g of O_2 and the ceria foam released 47 and 51 µmol/g of O_2. The CO production yields were 94 and 98 µmol/g with the ceria powder, and 99 and 96 µmol/g with the ceria foam. No significant change was observed between the two cycles, except the kinetic of re-oxidation during the first cycle. The ceria foam presents a steep mass increase that is explained by the dual porosity of the foam that improves the kinetics of CO_2 splitting.

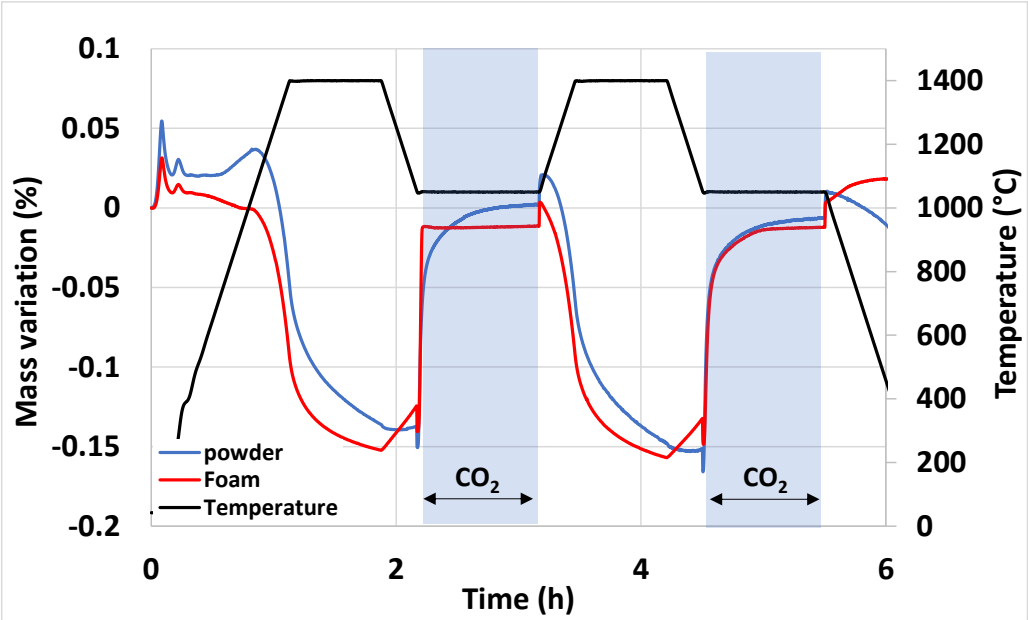

Figure 5. TGA of the commercial ceria powder and derived custom-made foam during two consecutive CO_2-splitting cycles.

A campaign of experimental solar tests was then carried out with the custom-made ceria foams shaped to fit the cavity of the solar reactor. A disc of 46 mm diameter and 17 mm high, and two rings of the same diameter and height were inserted into the solar reactor cavity (Figure 3). It represents a load of approximately 50 grams of active material.

3.2 Parametric study with the CeO_2 foams in the solar reactor

A parametric study was carried out with the aim of optimizing the production performance of solar fuel (H_2/CO). Consecutive cycles of CO_2 and H_2O dissociation were performed to study the effect of various operating conditions on fuel production rates and yields. The reduction temperature was set at 1400°C (T1) and the parametric study focused on various parameters including the pressure of the reduction step (P_{red}), the temperature of the oxidation step (T_{ox}), the total gas flowrate during oxidation (Q_{ox}), and the reactive gas concentration (CO_2/H_2O).

3.2.1 CO_2 dissociation cycles

Two series of CO_2-splitting cycling experiments were performed with the same foams (total loaded mass m = 50.02 g). Five consecutive cycles were realized during the first series and three consecutive cycles during the second one. Figure 6 presents the temperature profile of the foam near the bottom of the cavity (T1 in Fig. 2), the temperature measured by the pyrometer, and the evolution of gas species production rates (O_2 and CO). Note that gas rates are scaled with two different axes, otherwise the O_2 production rate profile would not be visible as its outlet concentration is much lower than the CO concentration (CO exhibits fast production rate whereas O_2 production profile is much longer). The values of peak production rates are reported in Table 2. The influence of several experimental parameters was investigated such as the total pressure during reduction, the oxidation temperature, and the CO_2 flowrate. For all experiments, the reduction temperature was set at 1400°C (T1) and argon was injected both in the window area ($Q_{Ar,top}$=1 NL/min) and at the top of the cavity from the side ($Q_{Ar,cavity}$=0.2 NL/min). The temperature measured by the pyrometer was ~70-100°C higher during heating and dwells, thus revealing a temperature gradient inside foams along the height. The average temperature of the foam was thus above 1400°C and was between the temperature of the pyrometer and T1. Reaching a perfectly homogeneous temperature through the foam heated by concentrated solar radiation is not possible, unlike conventional heating devices such as perfectly-controlled electric ovens. Since the ceria reduction process is highly sensitive to temperature, which greatly affects the extent of oxygen non-stoichiometry δ, it should be noted that the specified reduction temperature of 1400°C was the control temperature at T1 but the top of the foam was above this temperature.

Table 2 reports the results of CO_2 splitting cycles for each experimental condition. During the three first cycles, the O_2 production yield reached 97, 100, and 99 µmol/g (δ ~ 0.034) for a total pressure of 870 mbar (atmospheric pressure in Odeillo laboratory in Pyrenees mountains) during the reduction step. This reduction yield was well reproducible during cycles #1, #2, and #3, all carried out under the same experimental conditions (Q_{Ar}=1.2 NL/min, T_{red}=1400°C). Since the controlled temperature (T1) was located near the foam bottom, the upper part of the material was actually above this temperature (as denoted by the pyrometer measurement). Due to this temperature gradient, the global reduction

yield was higher than the one measured in TGA. The associated CO production yield, with CO_2 injection starting at 1000°C during cooling, was 245, 229, 226 µmol/g for cycle #1, #2, #3 with peak production rates of 3.3, 2.3, and 3.5 mL/min.g, respectively. The lower peak production rate during cycle #2 is due to a lower cooling rate during the oxidation step, as observed in Figure 6. These production rates and yields are consistent with previously reported values for ceria foams [36].

By decreasing the total pressure during the reduction step at 292 mbar (cycle #5) and 103 mbar (cycle #4), the oxygen partial pressure was decreased and the O_2 yield was significantly improved up to 123 µmol/g ($\delta \sim 0.042$) and 151 µmol/g ($\delta \sim 0.052$) respectively, while the associated CO production yields reached 271 µmol/g and 321 µmol/g, respectively. The CO peak production rate was also improved (3.9 mL/min.g and 4.7 mL/min.g, respectively) when the reduction yield was increased (Figure 7).

During cycles #6 to #8, pure CO_2 (mole fraction = 1) was injected at a different flowrate of 2 NL/min (instead of 1 NL/min). The CO production yield reached 332 µmol/g in cycle #6, 318 µmol/g in cycle #7, and 315 µmol/g in cycle #8 after a reduction step at 100 mbar (with $\delta \sim 0.052$-0.056). This confirms the repeatability and stability of the reactor performance. The CO production yield did not depend on the CO_2 flowrate (comparison between cycles #4 at 1 NL/min and #7 at 2 NL/min), but the peak production rate was improved by injecting higher CO_2 flowrates (8.2 mL/min.g for cycle #7 instead of 4.7 mL/min.g for cycle #4). The maximum CO production rates were 8.5 mL/min.g for a CO_2 injection temperature of 1000°C (cycles #6) and 10.2 mL/min.g for an injection temperature of 900°C (cycle #8).

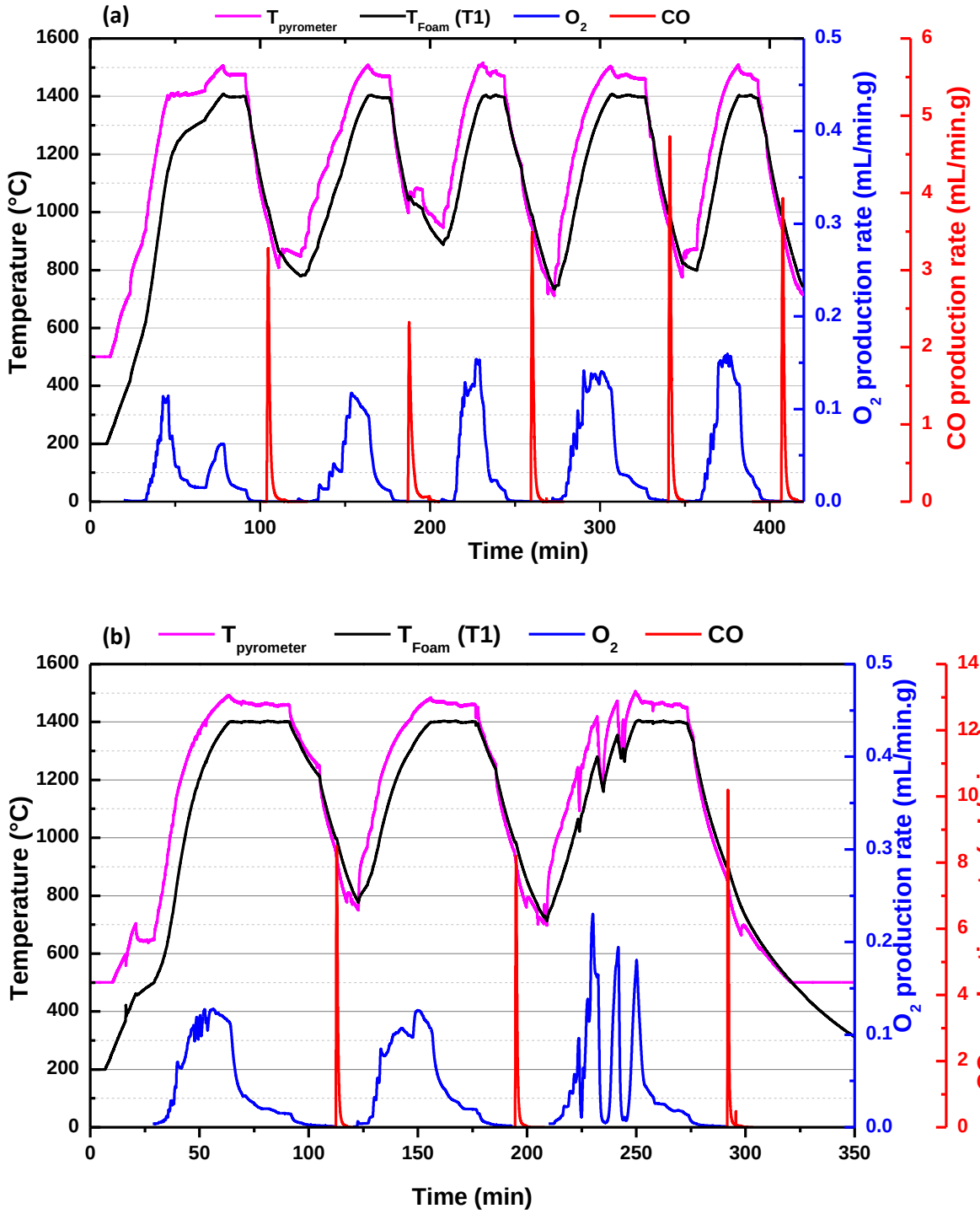

Figure 6. Temperature profiles and gas production rate evolution during CO_2-splitting solar cycles with CeO_2 foams: (a) cycles #1-5: influence of P_{red} (T_{ox}<1000°C and CO_2 flowrate = 1 NL/min), (b) cycles #6-8: influence of T_{ox} (P_{red}=100 mbar and CO_2 flow rate = 2 NL/min).

Table 2. Experimental conditions and results of CO_2-splitting solar cycles with CeO_2 foams (m = 50.02 g).

Cycle #	Reduction pressure (mbar)	CO_2 flowrate (NL/min)	Oxidation temperature start (°C)	O_2 yield ($\mu mol/g_{ceria}$)	CO yield ($\mu mol/g_{ceria}$)	CO peak production rate (mL/min.g)	CO/O_2 ratio
Cycle 1	874	1	1000	96.9	244.7	3.3	2.5
Cycle 2	879	1	1000	100.2	228.5	2.3	2.3
Cycle 3	879	1	1000	98.6	226.1	3.5	2.3
Cycle 4	103	1	1000	150.6	320.5	4.7	2.1
Cycle 5	292	1	1000	123.3	270.9	3.9	2.2
Cycle 6	100	2	1000	161.8	332.3	8.5	2.1
Cycle 7	100	2	1000	151.9	318.4	8.2	2.1
Cycle 8	100	2	900	155.5	314.7	10.2	2.0

This experimental study demonstrates the relevant cyclability of ceria foams, thus offering good repeatability of CO production. Favourable conditions for increasing CO production are a decrease in total pressure during the reduction step (decrease of p_{O2}), an increase in CO_2 flowrate and a decrease of re-oxidation temperature. Such conditions enhance CO production but can have a negative impact on energy efficiency as (i) higher gas flowrates result in higher energy consumption for heating, (ii) a reduction step at low pressure implies pumping work, and (iii) lowering the temperature during the oxidation step results in sensible heat losses when considering the full cycle.

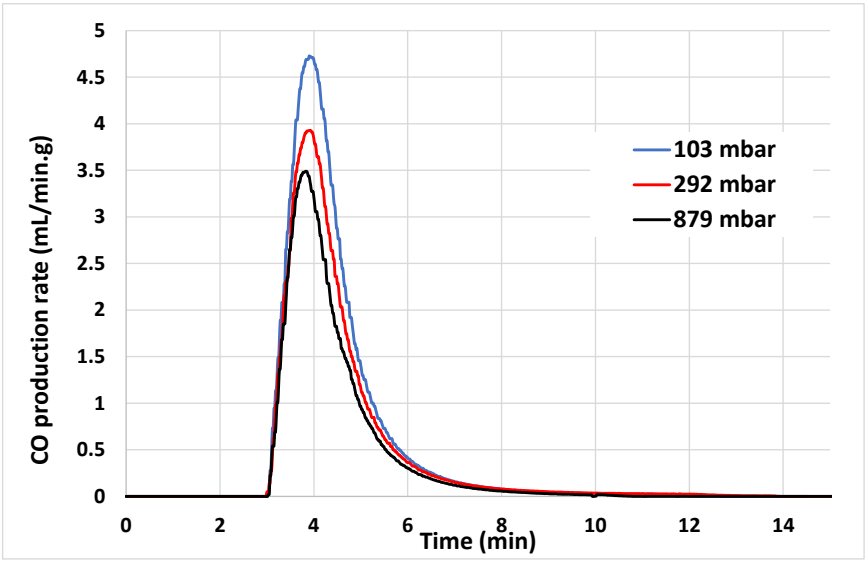

Figure 7. CO production rate evolution for three different total pressures during the reduction step (cycles #3-5, T_{ox}<1000°C, 1 NL/min CO_2 flowrate)

3.2.2 Water dissociation cycles

Two series of H_2O-splitting solar cycling experiments were also realized with the same foams (total loaded mass m = 50.02 g). Several experimental parameters were investigated such as the total pressure during reduction, the total Ar carrier gas flowrate during hydrolysis, and the steam content. Table 3 presents the selected experimental conditions for the reduction and oxidation steps, as well as the results of O_2 and H_2 production. Figure 8 shows the temperature profiles and gas production rates during the 8 thermochemical cycles.

Table 3. Experimental conditions and results of H_2O-splitting solar cycles with CeO_2 foams (m = 50.02 g).

Cycle #	Reduction pressure (mbar)	Argon flowrate (hydrolysis-NL/min)	H_2O mole fraction	O_2 yield (µmol/g_{ceria})	H_2 yield (µmol/g_{ceria})	H_2 peak production rate (mL/min.g)	H_2/O_2 ratio
Cycle 1'	868	1.0	29.4%	101.2	203.6	1.5	2.01
Cycle 2'	904	1.0	38.4%	105.4	202.9	1.9	1.93
Cycle 3'	899	1.0	45.4%	105.1	199.0	2.2	1.89
Cycle 4'	103	1.0	45.4%	148.5	280.6	3.0	1.89
Cycle 5'	904	1.0	51.0%	99.8	187.0	2.2	1.87
Cycle 6'	905	1.0	55.5%	97.6	176.9	2.5	1.81
Cycle 7'	902	1.5	35.7%	98.4	182.3	2.2	1.85
Cycle 8'	905	2.0	29.4%	97.3	188.0	2.4	1.93

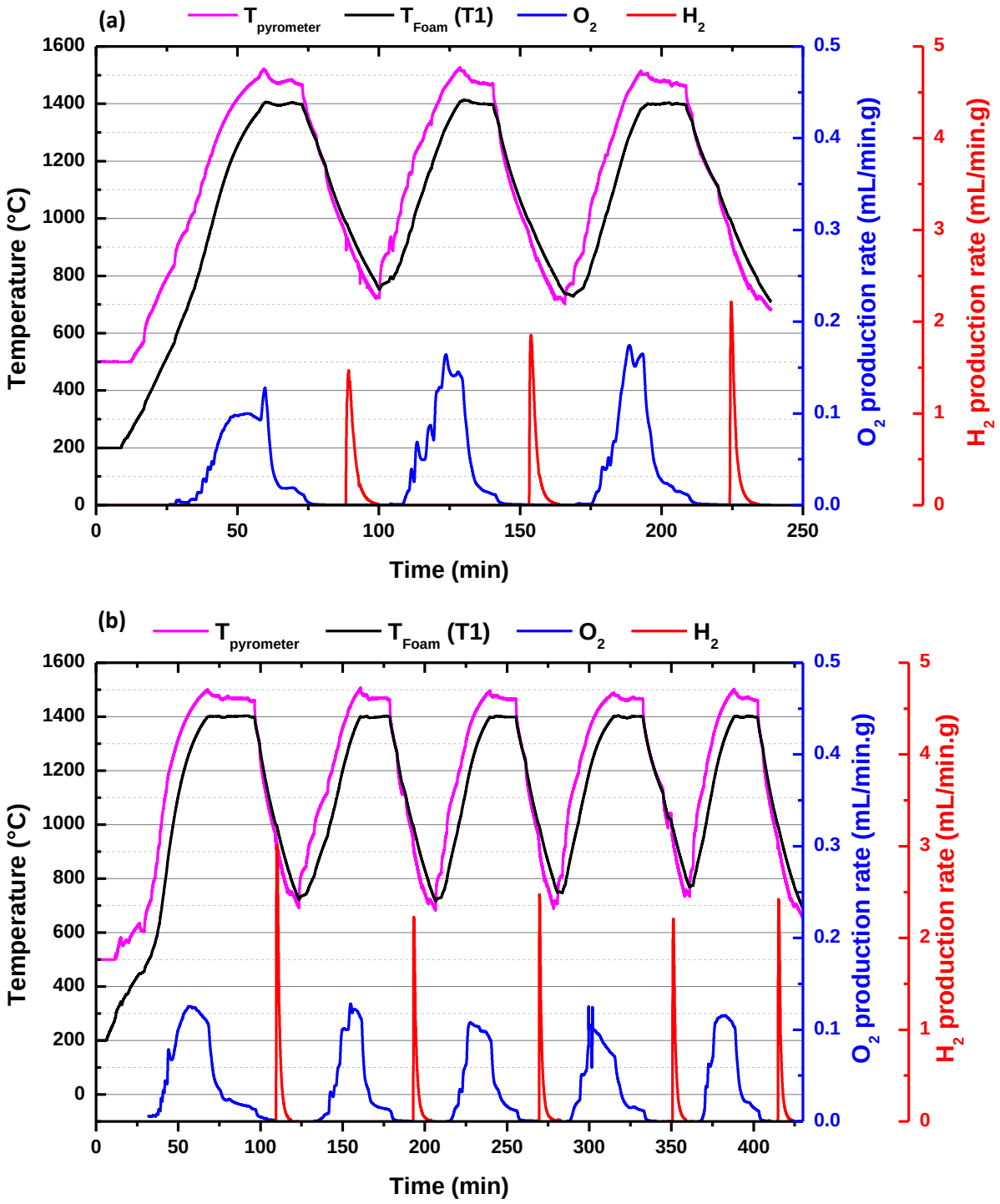

Figure 8. Temperature profiles and gas production rate evolution during H_2O-splitting solar cycles with CeO_2 foams: (a) cycles #1'-3': influence of H_2O mole fraction, (b) cycles #4'-8': influence of reduction pressure (P_{red}) and Ar flow rate during oxidation.

The highest H_2 production yield was 280.6 µmol/g_{ceria} during cycle #4' with a low-pressure reduction step (103 mbar), a hydrolysis step at T_{ox}<1000°C, and a steam content in the sweep gas of 45.4%. The highest H_2 production rate was 3.0 mL/min.g_{ceria} that was obtained during the same cycle. This peak rate is lower than in the case of CO_2 because pure CO_2 was used, whereas Ar was used as carrier gas during H_2O injection, which lowered the steam content in the oxidation step. The optimal parameters to improve the H_2 production are a low-pressure reduction step, a high steam content, and a high gas flowrate during the hydrolysis step. The rate of the hydrolysis step is directly related to the steam content.

Figure 9 illustrates the influence of the steam content in the sweep gas during hydrolysis at the same temperature (T_{ox}<1000°C) and Ar flowrate (1 NL/min). The higher the steam content, the higher the H_2 peak production rate. The steam content only impacts the hydrolysis rate while overall O_2 and H_2 yields remain unchanged. This is because the oxidation step is complete regardless of the steam content. Increasing the Ar flowrate during hydrolysis (cycles #6',7',8') decreases the H_2O mole fraction but this effect does not impact H_2 production rates and yields. Indeed, the increase in the total gas flow rate promotes the mass transfer of gas species, decreases the molar fraction of H_2 (thereby shifting the reaction equilibrium towards H_2), and further sweeps the H_2 produced away from the reaction sites, which in turn promotes the hydrolysis reaction.

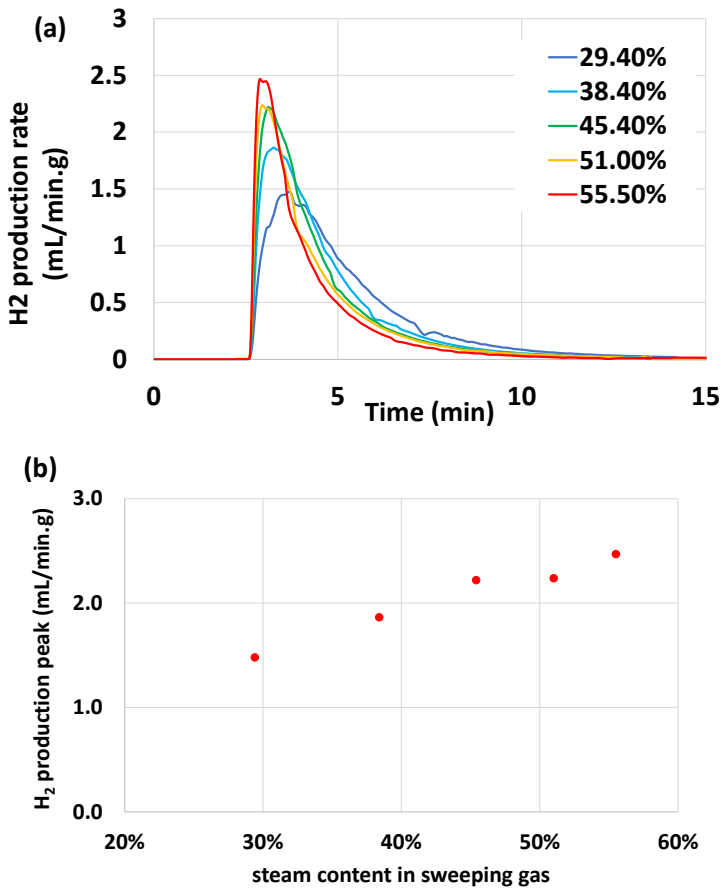

Figure 9. (a) H_2 production rate evolution and (b) peak production rate as a function of steam content in the sweep gas (cycles #1', 2', 3', 5', 6': reduction step at T1 = 1400°C and other hydrolysis parameters unchanged).

Figure 10 compares the production yields of CO and H_2 by solar thermochemical cycles with ceria foams over the entire solar experimental series. The cycling capability is highlighted as no deactivation was observed regarding O_2 release during the reduction steps. About 100 µmol/g of O_2 was released during reduction steps at T1 = 1400°C under a total pressure of ~900 mbar. The dissocation of CO_2 appears to be more efficient than H_2O splitting, which is mainly the result of the different concentration of oxidant gas during the oxidation step. Indeed, a pure CO_2 stream was used while no experiment could be conducted with pure steam injection due to technical constraints.

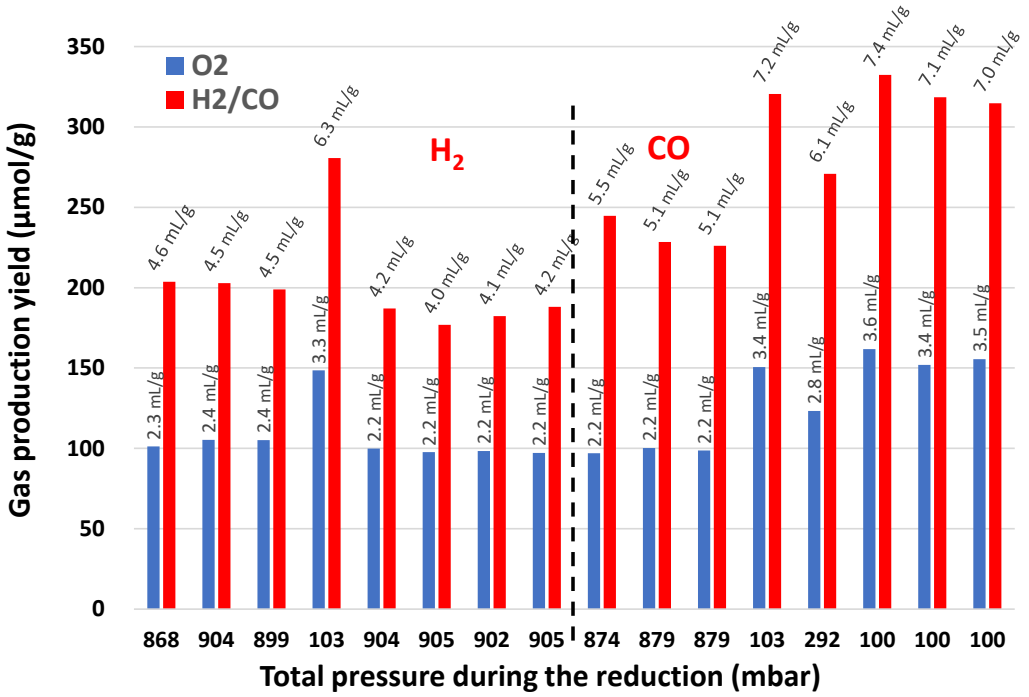

Figure 10. Comparison of O_2 and CO/H_2 production yields during 16 consecutive solar thermochemical cycles using ceria foams and different experimental conditions.

3.2.3 Simultaneous H_2O and CO_2 dissociation cycles for syngas production

In order to complete the on-sun experimental campaign with ceria foams, simultaneous CO_2- and H_2O-splitting cycles were performed to produce syngas. The reduction steps were carried out under low pressure (115 mbar) with a flow of Ar (1.2 NL/min), and the oxidation steps were carried out at T_{ox}<1000°C with 41% steam (50 g/h), 39% CO_2 (1 NL/min), and 20% Ar (0.5 NL/min) as sweep gas composition (Table 4). Steam and CO_2 flowrates were chosen to have a similar concentration in the flowing gas and to not favour one reaction over another when simultaneous splitting. Three consecutive splitting cycles were performed and Figure 11 shows the temperature profiles and gas production rates. The maximum production rate of CO was higher than H_2 with respectively 4.6, 3.8, and 3.2 mL/min.g and 1.7, 1.4, 2.2 mL/min.g (Table 4).

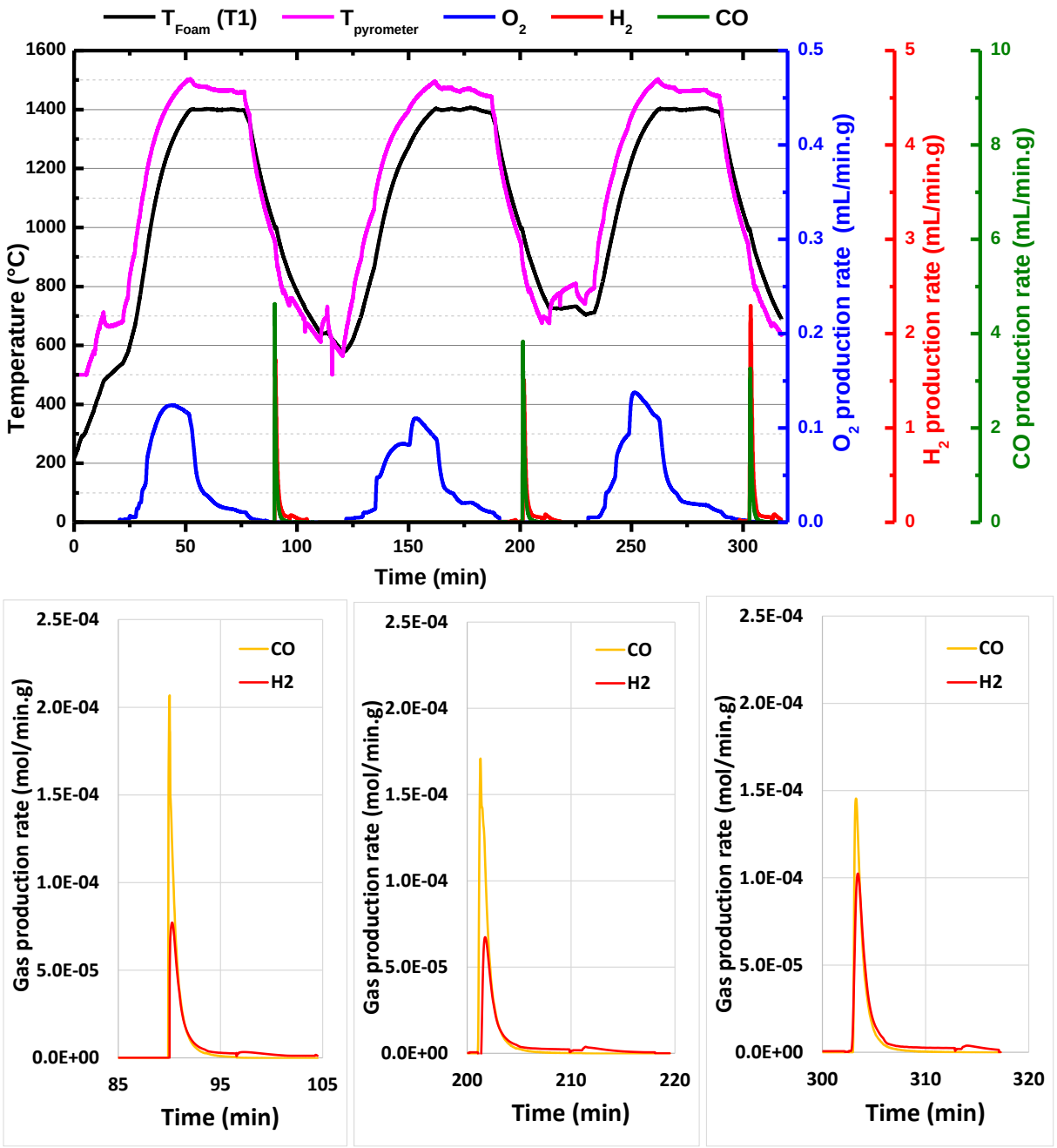

Figure 11. Temperature profiles and gas production rate evolution during simultaneous CO_2- and H_2O-splitting solar cycles with CeO_2 foams: (top) overall successive cycles, (bottom) zoom on CO and H_2 production peaks (cycles #1"-3").

Figure 12 shows the cumulative production yields of O_2 during the reduction steps and of CO and H_2 during the reoxidation steps. The O_2 amounts released during low pressure (115 mbar) reduction steps at T1 = 1400°C reached 137, 137, and 145 µmol/g for the three consecutive cycles (Table 4). During the

first and second cycles, the CO production yield was higher than the H_2 production yield (144.6 and 160.7 µmol/g for CO against 114.7 and 111.9 µmol/g for H_2). In contrast, during the third cycle, the production of H_2 was higher than the production of CO (159.0 and 138.5 µmol/g, respectively). This trend could be explained by the difference in reactive gas injection time. Indeed, the first gas species entering the cavity react first preferably with the surface sites of the ceria foams, and it is experimentally difficult to control which one will enter the reactor first. A very short delay in oxidant gases injection (small lag between H_2O and CO_2 injections) results in a significantly different syngas composition. Operating perfectly simultaneous gases injection is challenging and may represent a process limitation when co-feeding H_2O and CO_2 for H_2:CO ratio control. Direct syngas production by co-feeding of H_2O and CO_2 did not turn to be advantageous for precise control of the syngas composition. Nevertheless, the sum of CO and H_2 production yields lead to full reoxidation extent with a ($CO+H_2/O_2$) ratio equal to 1.9 or 2.

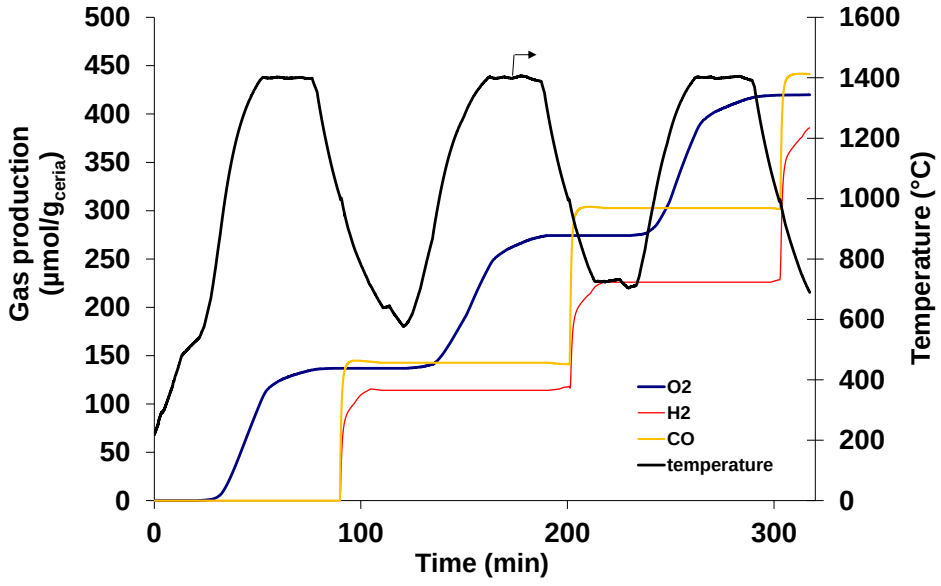

Figure 12. Cumulative gas production evolution (O_2 and syngas) and temperature profile for three consecutive thermochemical cycles operated on-sun with CeO_2 porous foams

Table 4. Results of simultaneous CO_2- and H_2O-splitting solar experiments with CeO_2 foams (m = 64.1 g).

Cycle #	O_2 (µmol/ g_{ceria})	CO yield (µmol/g_{ceria})	CO maximum production rate (mL/g.min)	H_2 yield (µmol/ g_{ceria})	H_2 maximum production rate (mL/g.min)	CO + H_2 (µmol/g_{ceria})	(CO+H_2)/O_2
Cycle 1"	136.9	144.6	4.6	114.7	1.7	259.3	1.9
Cycle 2"	137.4	160.7	3.8	111.9	1.4	272.6	2.0
Cycle 3"	145.3	138.5	3.2	159.0	2.2	297.5	2.0

3.3 Effect of total loaded mass of ceria foams

The amount of fuel produced per cycle can be further improved by increasing the total amount of reactive ceria loaded in the reactor cavity. Redox cycles were carried out with a higher charge of ceria foams (72.9 g) in the solar reactor to optimize fuel yield and analyse the energy balance. This was achieved by preparing ceria foams with higher bulk density and increasing the number of stacked rings to fully fill the volume of the reactor cavity (a bottom disc and three rings were used in this case). The goal was to utilize the reactor's maximum loading potential to optimize the reactor's fuel production capacity. Two consecutive CO_2 splitting cycles were carried out with a reduction step at low-pressure (105 mbar) and an oxidation step at T_{ox}<1000°C with 66% CO_2 gas flowing into the cavity (2 NL/min CO_2 and 1 NL/min Ar). In addition, two H_2O splitting cycles were carried out with low-pressure during reduction first (105 mbar) and atmospheric pressure (900 mbar). The oxidation steps were operated at T_{ox}<1000°C and T_{ox}<900°C with 60 g/h H_2O and 1 NL/min Ar.

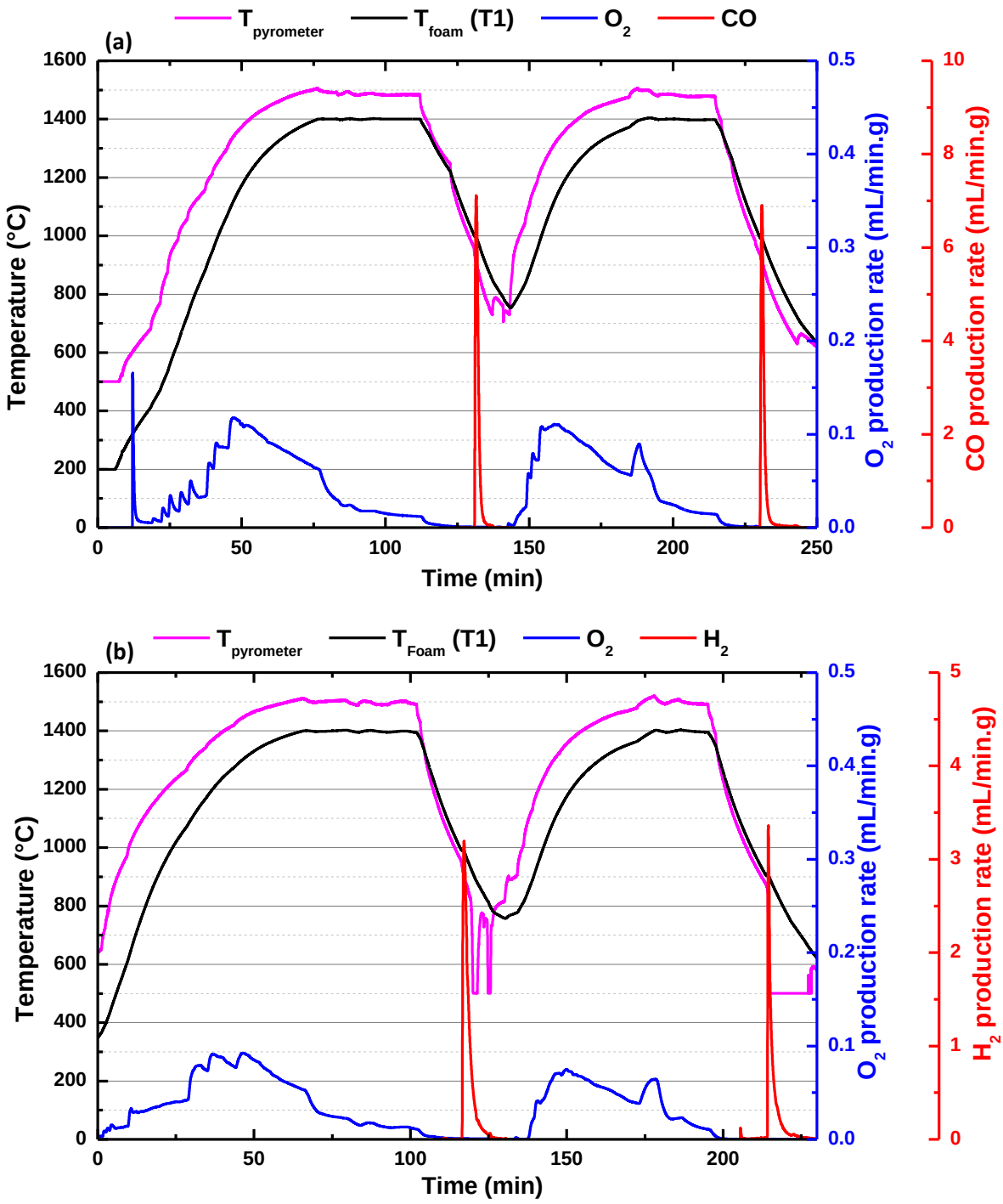

Figure 13. Temperature profiles and gas production rate evolution during (a) CO_2-splitting and (b) H_2O-splitting solar cycles with maximized loading of CeO_2 foams (m = 72.9 g) in the solar reactor.

Table 5 presents the O_2 and CO/H_2 yields produced during these cycles. The quantities of O_2 produced during the reduction steps were higher than the previous values measured under the same conditions (212.5, 198.9, and 198.1 µmol/g at 105 mbar and 116.0 µmol/g at 900 mbar). The δ values were thus also higher (maximum δ ~ 0.073 in cycle #1'''). This is explained by the larger amount of ceria placed

in the cavity and the different total height. Indeed, a disc and three rings of ceria foams were inserted in the cavity and the first ring was located at the top of the cavity directly heated by concentrated solar radiation. Therefore, the topmost ring was heated to a higher temperature even though the temperature profile of T1 and the pyrometer did not show such temperature increase at the top of the cavity compared to previous experiments. CO production reached 408.5 and 404.0 µmol/g during the oxidation steps (representing 9.1 and 9.0 mL/g) and the H_2 production yields reached 314.3 and 204.8 µmol/g. These amounts of CO and H_2 overpass the previous values measured under the same conditions, which were respectively 332.3 µmol/g (cycle #6 in Table 2) and 280.6 µmol/g (cycle #4' in Table 3 at low pressure and T_{ox}<1000°C). The CO:O_2 ratio was 1.9 and 2.0, which confirms a total re-oxidation of the reduced ceria by CO_2, whereas the H_2:O_2 ratio was 1.6 and 1.8, which denotes a partial re-oxidation of reduced ceria with water. This can be explained by the steam injection inlet which is placed on the side of the cavity at a height lower than the topmost ceria ring. Therefore, the steam was not distributed over the top of the cavity because the sweep gas (Ar) flows from the top and carries the steam down. This phenomenon was not observed with CO_2 because it was injected both from the top and from the side of the cavity. The total amounts of CO produced during the two cycles were 667 mL and 659 mL, respectively, while the total amounts of H_2 produced per cycle were 458 mL and 334 mL. Optimization of the fuel production capacity was thus successfully achieved by maximizing the total amount of ceria foam loaded into the reactor.

Table 5. Results of CO_2- and H_2O-splitting cycles with 72.9 g of ceria foams in the solar reactor.

Cycle #	Reduction pressure (mbar)	CO_2 or H_2O mole fraction	O_2 (µmol/g_{ceria})	CO (µmol/g_{ceria})	CO maximum production rate (mL/g.min)	H_2 (µmol/g_{ceria})	H_2 maximum production rate (mL/g.min)	(CO or H_2)/O_2
Cycle 1"'	105	66%	212.5	408.5	7.1	-	-	1.9
Cycle 2"'	105	66%	198.9	404.0	6.9	-	-	2.0
Cycle 3"'	105	55.5%	198.1	-	-	314.3	3.2	1.6
Cycle 4"'	900	55.5%	116.0	-	-	204.8	3.4	1.8

			(T_{ox}< 900°C)

Figure 14 presents SEM pictures of a ceria foam before and after thermochemical cycling under concentrated solar radiations. It is observed that the thickness of ceria strands does not change after thermal cycling (Fig. 14 right). Cylindrical pores of 8 µm diameter and 80 µm long are observed in both cases. Nevertheless, the material seems to slightly densify after thermochemical cycling. The ceria grain size is also increased after thermal cycling (unlike the crystallite size that remains unchanged according to XRD, Fig. 4). The grains grow from 5 µm to 20 µm. A grain can be composed of several crystallites (crystalline domains). Grain growth is observed by SEM due to agglomeration of crystallites. These observations confirm the good thermal stability of the developed porous ceria foams under concentrated solar energy and demonstrate that grain growth has no influence on CO_2 and H_2O splitting rates and yields.

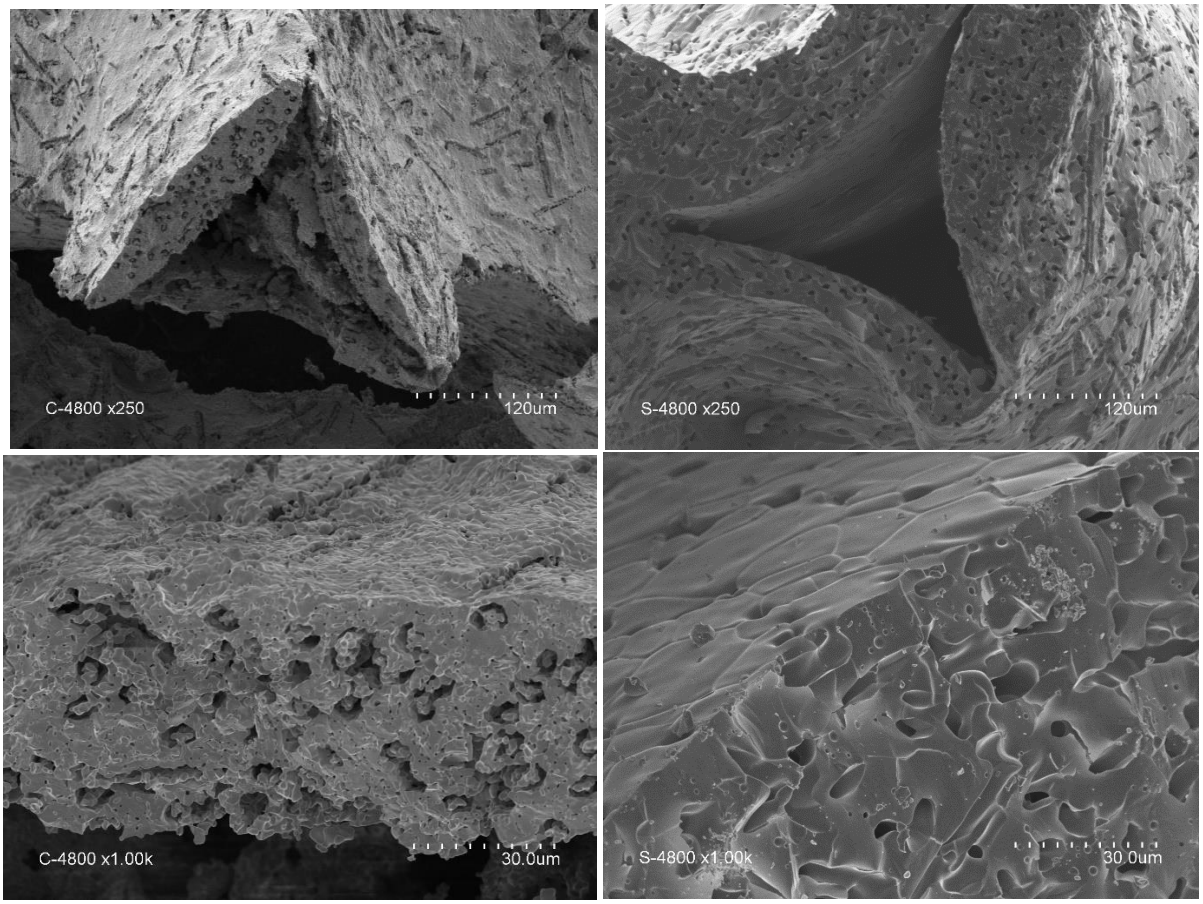

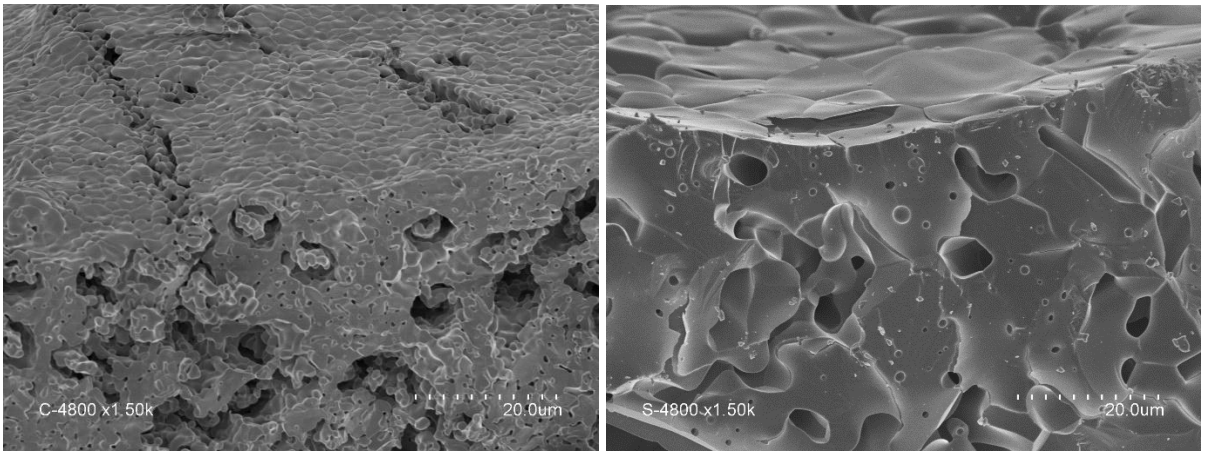

Figure 14. SEM pictures of a ceria foam before (left) and after (right) the whole series of solar CO_2 and H_2O thermochemical cycles at 1400°C.

The solar-to-fuel efficiency during the peak production (real-time efficiency) can be calculated by the following equation [16]:

$$\eta_{solar\text{-}to\text{-}fuel}=F_{fuel}.HHV_{fuel}/P_{solar} \quad (3)$$

where F_{fuel} denotes the CO or H_2 production rate (mol/s), HHV_{fuel} the higher heating value of CO (= 283 kJ/mol) or H_2 (= 286 kJ/mol), and P_{solar} the maximum solar power input during the reduction step (kW). Such real-time efficiency eliminates the influence of arbitrary process conditions such as the duration of the reduction step or the effect of weather conditions. Auxiliary power inputs are not taken into account such as pumping works, inert gas regeneration, solar tracking, etc.

P_{solar} only relates to the reduction step because no heating was applied during the oxidation step (free cooling). Table 6 reports the results of the solar-to-fuel efficiency calculations with 72.9 g of ceria foams. CO_2-splitting cycles are more efficient compared to H_2O-splitting cycles with peak solar-to-fuel efficiencies of 10.1% and 9.8% for CO_2 splitting against 4.5% and 4.9% for H_2O splitting. These values are higher than the previously reported ones. For example, Haeussler et al [36] reported a solar-to-fuel efficiency of 7.5% for CO_2 splitting in the same reactor (P_{red}=110 mbar, T_{Ox}=900°C, Q_{CO2}=2 NL/min), but with different ceria foams. When considering the total solar energy input integrated over the reduction step duration, an average energy efficiency can be estimated. However, such an efficiency is strongly dependent (inversely proportional) on the duration of the reduction step which can be

artificially lowered by using high heating rates, in turn drastically increasing the efficiency. This duration is thus arbitrary and depends on the applied experimental protocol. This is typically the case in reactors using an electrical heating source (Xe-lamp based simulators) with facile control of heating rate, which thus artificially boosts the efficiency. Accordingly, the reduction step duration was commonly kept extremely short [21] and consisted in heating the material very fast up to 1500°C and stopping immediately the heating (thus not applying any temperature dwell at the maximum temperature) although the oxygen release equilibrium was not reached. As a result, the whole duration was less than 10 min in [21] thus minimizing the amount of energy consumed and yielding 5.25% efficiency, compared with ~50-70 min (with varying solar power input) in the present study yielding ~0.3-0.5% efficiency. In summary, when aiming to reduce the amount of solar energy consumed while increasing the efficiency, the reduction step duration can be shortened by (i) using fast heating up to higher temperatures (e.g., 1500°C) to enhance the reduction extent, and (ii) stopping the solar power input before waiting for complete equilibrium without significantly affecting the amount of oxygen produced. However, beyond the efficiency the most important metrics of the material and process performance are rather the fuel production rates and global fuel yields per unit mass of reactive material. This study showed that improving solar fuel production performance was possible by suitable tuning of material structure and process conditions.

In summary, the main novel outputs raised by the study are the followings:

- A reactive material for redox cycling was prepared as reticulated porous foams with improved morphology and microstructure suitable for solid-gas reactions and solar radiation absorption. In particular, foams with dual-scale porosity were obtained by using the replication method thanks to the addition of filamentous pore formers in the slurry.

- The reticulated foams were cycled in a solar reactor to determine the fuel production performance under realistic conditions, with continuous online monitoring of the evolved gas species produced during reaction steps. A sensitivity study of the fuel production rates on various operating parameters

was performed including pressure during reduction, temperature during oxidation, oxidant mole fraction or oxidant gas flow-rate.

- Both CO_2 and H_2O splitting were investigated to assess the influence of the oxidizing gas. In addition, co-feeding of H_2O and CO_2 for direct syngas production was also considered.

- Material cyclability was checked over several consecutive cycles for splitting CO_2 and H_2O to demonstrate performance stability.

- The amount of loaded material in the reactor was optimized to maximize the fuel production capacity.

- Remarkably high fuel production rates and yields were obtained thanks to the methods employed to improve materials and solar thermochemical conversion outcomes.

Table 6. Solar-to-fuel efficiency calculations with high load of ceria foams in the solar reactor.

Cycle #	F_{fuel} (mL/g.min)	F_{fuel} (mol/s)	HHV_{fuel} (kJ/mol)	P_{solar} (W)	$\eta_{solar\text{-}to\text{-}fuel}$ (%)
Cycle 1"'	7.1	385.10^{-6}	283	1078.1	10.1
Cycle 2"'	6.9	374.10^{-6}	283	1078.6	9.8
Cycle 3"'	3.2	174.10^{-6}	286	1113.0	4.5
Cycle 4"'	3.4	184.10^{-6}	286	1079.9	4.9

4. Conclusion

A complete study was reported ranging from the synthesis of reactive materials in the form of customized foams with a porous structure in the struts, to their application in a two-step solar thermochemical process for fuel production, with optimization of the process conditions and solar reactor operation. Dual-scale porous ceria foams (10 ppi reticulated foams with micrometer-scale pores inside struts) were synthesized and employed in a solar cavity reactor for CO_2 and H_2O thermochemical splitting. Optimization of cycling parameters and reactor operation was performed to maximize the fuel productivity and efficiency with the customized redox-active material in the form of reticulated porous structure. More than 20 cycles were carried out to optimize fuel production

performance based on several experimental parameters such as total pressure, temperatures, oxidant content or gas flowrates. Stable cycling performance for consecutive H_2O and CO_2 splitting was demonstrated. The on-sun experiments revealed enhanced fuel production rates and yields with high performance stability. Maximum CO and H_2 production yields of 332 µmol/g and 281 µmol/g were obtained after a reduction step at 1400°C under a reduced total pressure of 100 mbar. Peak rates of 10.2 mL/min.g and 3.0 mL/min.g were measured during CO and H_2 production steps, respectively. Lower H_2 production rates were evidenced due to the lower steam content compared to the case of CO_2 injection (pure CO_2 was used). This explains the lower production rates obtained when feeding steam instead of CO_2. Solar syngas production was further evidenced by a simultaneous CO_2 and H_2O dissociation. Precise tuning of syngas composition remains however challenging given the difficulty to perfectly synchronise gases injection when co-feeding H_2O and CO_2. Finally, high loading of ceria foams in the solar reactor enabled to increase the amount of both CO and H_2 produced per cycle (667 mL and 513 mL, respectively) with fairly good solar-to-fuel efficiencies at lab-scale (10.1% and 4.9%, respectively). This work demonstrates that solar fuels production can be enhanced by using custom-made ceria foams under real solar conditions, thus opening the road towards efficient solar thermochemical processes competing favourably with conventional electrochemical processes.

Acknowledgements

This research was partially funded by H2VERT project led by Région Occitanie in France (Défi clé Hydrogène Vert- Plan de relance - FEDER REACT EU - Hydrosol sub-project). The authors thank Marielle Vallès for her internship contribution in microscopy to this project.

References

[1] Lhyfe inaugurates world's first industrial site for renewable green hydrogen, Fuel cells bulletin, 2021, 11, 2021

[2] Rodler A, Haurant P, Faggianelli G, Pigelet G, Poggi P. Combined heat and power generation of the hydrogen chain based on MYRTE platform. Solar World Congress 2015. International Solar Energy Society conference proceedings. 8-12, November 2015

[3] Funk J E. Thermochemical hydrogen production: past and present, International journal of hydrogen energy, 26, 3, pp.185-190, 2001

[4] Li X, Sun X, Song Q, Yang Z, Wang H, Duan Y. A critical review on integrated system design of solar thermochemical water-splitting cycle for hydrogen production, International journal of hydrogen energy, 47, 79, pp.33619-33642, 2022

[5] Yadav D, Banerjee R. A review of solar thermochemical processes, Renewable and sustainable energy reviews, 54, pp.497-532, 2016

[6] Safari F, Dincer I. A review and comparative evaluation of thermochemical water splitting cycles for hydrogen production, Energy conversion and management, 205, 112182, 2020

[7] Abanades S. Metal oxides applied to thermochemical water splitting for hydrogen production using concentrated solar energy, Chem Engineering, 3, 63, 2019

[8] Mao Y, Gao Y, Dong W, Wu H, Song Z, Zhao X, Sun J, Wang W. Hydrogen production via a two-step splitting thermochemical cycle based on metal oxide-A review, Applied Energy, 267, 114860, 2020

[9] Carrillo R, Scheffe J. Advances and trends in redox materials for solar thermochemical fuel production, Solar Energy, 156, pp.3-20, 2017

[10] Bulfin B, Vieten J, Agrafiotis C, Roeb M, Sattler C. Applications and limitations of two-step metal oxide thermochemical redox cycles; A review, Journal of Materials Chemistry A, 5, 18951-18966, 2017

[11] Wim H, Geerlings H. Efficient production of solar fuel using existing large scale production technologies, Environmental science technology, 45, pp.8609-8610, 2011

[12] Kim J, Johnson T, Miller J, Stetchel E, Maravelias C. Fuel production from CO2 using solar-thermal energy: system level analysis, Energy and environmental science, 5, pp.8417-8429, 2012

[13]Schappi R, Rutz D, Dahler F, Muroyama A, Haueter P, Lilliestam J, Patt A, Furler P, Steinfeld A. Drop-in fuels from sunlight and air, Nature, 601, pp.63-68, 2022

[14]Zoller S, Koepf E, Nizamian D, Stephan M, Patane A, Haueter P, Romero M, Gonzales-Aguilar J, Lieftink D, de Wit E, Brendelberger S, Sizmann A, Steinfeld A. A solar tower fuel plant for the thermochemical production of kerosene from H2O and CO2, Joule, 6, pp.1606-1616, 2022

[15]Welte M, Barhoumi R, Zbinden A, Scheffe J, Steinfeld A. Experimental demonstration of the thermochemical reduction of ceria in a solar aerosol reactor. Ind Eng Chem Res, 55, 10618–25, 2016

[16]Ermanoski I, Siegel N, Stechel E. A new reactor concept for efficient solar-thermochemical fuel production. J Sol Energy Eng, 135, 031002, 2013

[17]Kaneko H, Miura T, Fuse A, Ishihara H, Taku S, Fukuzumi H, et al. Rotary-type solar reactor for solar hydrogen production with two-step water splitting process. Energy Fuels, 21, 2287–93, 2007

[18]Lapp J, Davidson J, Lipinski W. Heat transfer analysis of a solid-solid heat recuperation system for solar-driven nonstoichiometric redox cycles. J Sol Energy Eng, 135, 031004, 2013

[19]Agrafiotis C, Roeb M, Konstandopoulos A, Nalbandian L, Zaspalis V, Sattler C, et al. Solar water splitting for hydrogen production with monolithic reactors. Sol Energy, 79, 409–21, 2005

[20]Chueh W, Falter C, Abbott M, Scipio D, Furler P, Haile S, et al. High-flux solar-driven thermochemical dissociation of CO2 and H2O using nonstoichiometric ceria. Science, 330, 1797–801, 2010

[21]Marxer D, Furler P, Takacs M, Steinfeld A. Solar thermochemical splitting of CO2 into separate streams of CO and O2 with high selectivity, stability, conversion, and efficiency. Energy Environ Sci, 10, 1142–9, 2017

[22]Zhu L, Lu Y, Shen S. Solar fuel production at high temperatures using ceria as a dense membrane. Energy, 104, 53–63, 2016.

[23] Lou J, Tian Z, Wu Y, Li X, Qian X, Haile S, Hao Y. Thermodynamic assessment of nonstoichiometric oxides for solar thermochemical fuel production, Solar Energy, 241, pp.504-514, 2022

644 [24]Yang C, Yamazaki Y, Aydin A, Haile S. Thermodynamic and kinetic assessment of strontium-doped
645 lanthanum manganite perovskites for two-step thermochemical water splitting, J. Mater. Chem.,
646 2, pp.13612-13623, 2014
647 [25]Kim Y, Jeong S, Koo B, Lee S, Kwak N, Jung W. Study of the surface reaction kinetics of (La,Sr)MnO3
648 oxygen carriers for solar thermochemical fuel production, J. Mater. Chem., 6, p.13082-13089, 2018
649 [26]Lu Y, Zhu L, Agrafiotis C, Vieten J, Roeb M, Sattler C. Solar fuel production: two-step
650 thermochemical cycles with cerium-based oxides, Progress in energy and combustion science, 75,
651 pp.100785, 2019
652 [27]Marxer D, Furler P, Takacs M, Steinfeld A. Solar thermochemical splitting of CO2 into separate
653 streams of CO and O2 with high selectivity, stability, conversion, and efficiency, Energy Environ Sci.,
654 10, pp.1142–1149, 2017
655 [28]Kubicek M, Bork A, Rupp J. Perovskite oxides – a review on a versatile material class for solar-to-
656 fuel conversion process, Journal of materials chemistry A, 5, 11983-12000, 2017
657 [29]Bayon A, de la Calle A, Kamol Ghose K, Page A, McNaughton R. Experimental, computational and
658 thermodynamic studies in perovskites metal oxides for thermochemical fuel production: A review,
659 International journal of hydrogen energy, 45, 12653-12679, 2020
660 [30]Haeussler A, Abanades S, Jouannaux J, Julbe A. Non-stoichiometric redox active perovskite
661 materials for solar thermochemical fuel production: A review, Catalysts, 8, 611, 2018
662 [31]Zhai S, Rojas J, Ahlborg N, Lim K, Toney M, Jin H, Chueh W. Majumdar A. The use of poly-cation
663 oxides to lower the temperature of two-step thermochemical water splitting, Energy and
664 environmental science, 11, 2172-2178, 2018
665 [32]Gao Y, Mao Y, Song Z, Zhao X, Sun J, Wang W, Chen G, Chen S. Efficient generation of hydrogen by
666 two-step thermochemical cycles: Successive thermal reduction and water splitting reactions using
667 equal-power microwave irradiation and a high entropy material, Applied Energy, 279, 115777,
668 2020

669 [33]Gao Y, Zhang M, Mao Y, Cao H, Zhang S, Wang W, Sun C, Song Z, Sun J, Zhao X. Microwave-triggered
670 low temperature thermal reduction of Zr-modified high entropy oxides with extraordinary
671 thermochemical H2 production performance, Energy conversion and management, 252, 115125,
672 2022
673 [34]Luo J. New high entropy perovskite oxides with increased reducibility and stability for
674 thermochemical hydrogen generation, US DOE project review, 2020,
675 https://www.hydrogen.energy.gov/pdfs/review20/p194_luo_2020_p.pdf,
676 [35] Le Gal A, Valles M, Julbe A, Abanades S. Thermochemical properties of high entropy oxides used
677 as redox-active materials in two-step solar fuel production cycles, Catalysts, 12, pp.1116, 2022
678 [36]Haeussler A, Abanades S, Julbe A. Jouannaux J., Cartoixa B., Solar thermochemical fuel production
679 from H2O and CO2 splitting via two-step redox cycling of reticulated porous ceria structures
680 integrated in a monolithic cavity-type reactor, Energy, 201, 117649, 2020
681 [37]Orfila M, Sanz D, Linares M, Molina R, Sanz R, Marugan J, Botas J. H2 production by thermochemical
682 water splitting with reticulated porous structures of ceria-based mixed oxide materials,
683 International journal of hydrogen energy, 46, 17458-17471, 2021
684 [38]Cho H, Kodama T, Gokon N, Bellan S, Kim J. Development of synthesis and fabrication process for
685 Mn-CeO2 foam via two-step water splitting cycle hydrogen production, Energies, 14, 6919, 2021
686 [39]Hoes M, Ackermann S, Theiler D, Furler P, Steinfeld A. Additive-manufactured ordered porous
687 structures made of ceria for concentrated solar applications, Energy technology, 7, 1900484, 2019
688 [40]Haeussler A, Abanades S. Additive manufacturing and two-step redox cycling of ordered porous
689 ceria structures for solar driven thermochemical fuel production, Chemical engineering science,
690 246, 116999, 2021
691 [41]Furler P, Scheffe J, Marxer D, Gorbar M, Bonk A, Vogt U, Steinfeld A. Thermochemical CO2 splitting
692 via redox cycling of ceria reticulated foam structures with dual-scale porosities, Phys. Chem. Chem.
693 Phys., 16, pp.10503-10511, 2014

694 [42]Pullar R, Novais R, Caetano A, Barreiros M, Abanades S, Costa Oliveira F. A review of solar
695 thermochemical CO2 splitting using ceria-based ceramics with designed morphologies and
696 microstructures, Frontiers in chemistry, 7, 601,2019
697 [43]Abanades S, Haeussler A. Two-step thermochemical cycles using fibrous ceria pellets for H2
698 production and CO2 reduction in packed-bed solar reactor, Sustainable materials and technologies,
699 29, e00328, 2021
700 [44]Haeussler A, Abanades S, Costa Oliveira F A, Novais R, Pullar R. Solar redox cycling of ceria
701 structures based on fiber boards, foams and biomimetic cork-derived ecoceramics for two-step
702 thermochemical H2O and CO2 splitting, Energy and fuels, 34, pp.9037-9049, 2020
703 [45]Furler P, Scheffe J, Steinfeld A. Syngas production by simultaneous splitting of H2O and CO2 via
704 ceria redox reactions in a high temperature solar reactor. Energy & environmental science. 3,
705 pp.6098-6103, 2012
706 [46]Haeussler A, Abanades S, Julbe A, Ayral A, Cartoixa B. Remarkable performance of microstructured
707 ceria foams for thermochemical splitting of H2O and CO2 in a novel high-temperature solar reactor,
708 Chemical Engineering Research and Design, 156, pp.311-323, 2020
709 [47]Abanades S, Haeussler A, Julbe A. Synthesis and thermochemical redox cycling of porous ceria
710 microspheres for renewable fuels production from solar-aided water-splitting and CO2 utilization,
711 Applied physics letters, 119 (2), 023902, 2021
712 [48]Costa Oliveira F, Barreiros M, Haeussler A, Caetano A, Mouquinho P, Oliveira Silva R, Novais
713 A, Pullar R, Abanades S. High performance cork-templated ceria for solar thermochemical
714 hydrogen production via two-step water-splitting cycles, Sustainable Energy and Fuels, 4(6), pp.
715 3077–3089, 2020
716 [49]Costa Oliveira F, Barreiros M, Abanades S, Caetano A, Novais R, Pullar R. Solar thermochemical
717 CO2 splitting using cork-templated ceria ecoceramics, Journal of CO2 Utilization, 26, pp. 552–563,
718 2018

[50] Haeussler A, Abanades S, Jouannaux J, Drobek M, Ayral A, Julbe A. Recent progress on ceria doping and shaping strategies for solar thermochemical water and CO2 splitting cycles, AIMS Materials Science, 6(5), pp. 657–684, 2019

[51] Haeussler A, Abanades S, Julbe A, Jouannaux J, Cartoixa B. Two-step CO2 and H2O splitting using perovskite-coated ceria foam for enhanced green fuel production in a porous volumetric solar reactor, Journal of CO2 Utilization, 41, 101257, 2020

[52] Schwartzwalder K, Somers H, Somers V. Method of making porous ceramic articles, U.S.P office, 1963